Linear stability analysis of boundary layer over a long cylinder with rotation

Srikanth Derebail Muralidhar, Benoît Pier, Julian F. Scott, Rama Govindarajan

Linear stability analysis of boundary layer over a long cylinder with rotation

S. DEREBAIL MURALIDHAR[a], B. PIER[a], J. SCOTT[a], R. GOVINDARAJAN[b]

a. Laboratoire de mécanique des fluides et d'acoustique (CNRS—Université de Lyon), École centrale de Lyon, 36 avenue Guy-de-Collongue, F-69134 Écully, France.
srikanth.derebail@doctorant.ec-lyon.fr, benoit.pier@ec-lyon.fr

b. TIFR Centre for Interdisciplinary Sciences, Hyderabad, India

Résumé :

Cet article analyse la stabilité d'un écoulement axial sur un cylindre qui tourne autour de son axe. L'ecoulement de base est numériquement calculé à l'aide de l'approximation de couche limite. Puis l'analyse de stabilité linéaire permet de comprendre le mécanisme de déstabilisation et d'identifier la région de l'instabilité. L'effet de la rotation sur la stabilité temporelle est expliqué en utilisant une méthode perturbative.

Abstract :

This paper deals with the stability analysis of a cylinder which is rotating about its axis in an axial flow. The basic flow is numerically computed by using the boundary layer approximation. Then linear stability analysis elucidates the instability mechanism and also determines the region of instability. The effect of small rotation on temporal stability is explained using a perturbation method.

Keywords : Boundary layer, linear stability, critical curve, matrix perturbation method

1 Introduction

A three dimensional boundary layer develops when a semi-infinite rotating cylinder is placed in a uniform axial flow. The effect of curvature of the cylinder causes the boundary layer thickness to deviate from the classical Blasius solution. The addition of rotation results in a tangential velocity profile and also a pressure gradient in both radial and axial directions. This causes significant effect on the boundary layer characteristics. The linear stability analysis of such a steady flow provides information whether rotation stabilizes or destabilizes the flow and also helps to characterize the regions of instability in the flow. Rotating curved surfaces can be seen in wind turbine nose tips, airfoils etc. Hence it is important to understand the physical phenomena occurring in such a fundamental flow configuration.
The boundary layer over a flat plate was studied by Blasius (1908) where he computed the similarity solution for the flow and also obtained the skin friction. The boundary layer flow along a circular cylinder with an axial flow has been studied previously and the velocity profiles were given as power series

by Seban and Bond (1951). Glauert and Lighthill (1955) used asymptotic expansions to obtain the solution far downstream. The whole range of axial positions was covered by Jaffe and Okamura (1968) and they obtained the solution by using numerical methods. There have been some works on the linear stability analysis of axial flow along a cylinder. The instability mechanisms in non–rotating cylinders were explained by Tutty et al. (2002) and they have found that the flow is stable throughout the cylinder for a Reynolds number below 1060. The secondary instability analysis of non–rotating cylinder was studied by Vinod and Govindarajan (2012) and they have found that the flow remains stable to both primary and secondary disturbances at large axial distances. Herrada et al. (2008) have obtained the linear stability results for certain range of rotation rates. We have extended this work to first study the boundary layer characteristics of a rotating cylinder in an axial flow. Then the linear stability analysis is done to map out the regions of instability in the domain for large range of rotation. This paper also tries to explain the effect of small rotation on a cylinder in an axial flow using matrix perturbation theory.

2 Problem formulation

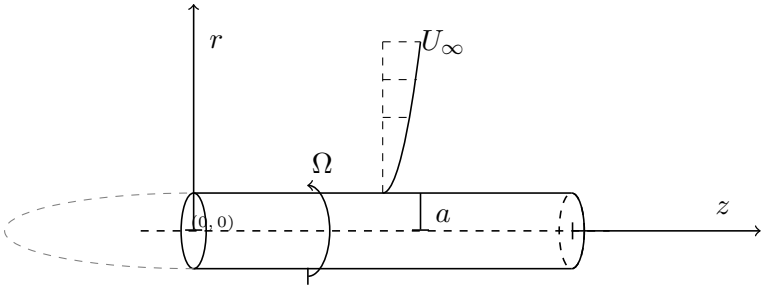

We consider a semi–infinite cylinder of radius a rotating at an angular velocity Ω about it axis. This cylinder is subjected to an incoming uniform flow with a free-stream velocity U_∞. Due to the no slip condition on the surface of the cylinder a boundary layer develops along the cylinder. It is assumed that there is a smooth nose before the cylinder to avoid any flow separation at the inlet. The Reynolds number is assumed to be sufficiently large so that the boundary layer on the nose is thin and has very small effect on the boundary layer development along the cylinder.
The following system is studied using 3-dimensional Navier–Stokes equations in cylindrical coordinates.

The velocities are non-dimensionalized by U_∞ and the radial and axial coordinates by radius a.

$$\frac{\partial u_z}{\partial t} + u_z\frac{\partial u_z}{\partial z} + u_r\frac{\partial u_z}{\partial r} + \frac{u_\theta}{r}\frac{\partial u_z}{\partial \theta} = -\frac{\partial p}{\partial z} + \frac{1}{Re}\left(\frac{\partial^2 u_z}{\partial r^2} + \frac{1}{r}\frac{\partial u_z}{\partial r} + \frac{1}{r^2}\frac{\partial^2 u_z}{\partial \theta^2} + \frac{\partial^2 u_z}{\partial z^2}\right), \tag{1}$$

$$\frac{\partial u_r}{\partial t} + u_z\frac{\partial u_r}{\partial z} + u_r\frac{\partial u_r}{\partial r} + \frac{u_\theta}{r}\frac{\partial u_r}{\partial \theta} - \frac{u_\theta^2}{r} = -\frac{\partial p}{\partial r} + \frac{1}{Re}\left(\frac{\partial^2 u_r}{\partial r^2} + \frac{1}{r}\frac{\partial u_r}{\partial r} + \frac{1}{r^2}\frac{\partial^2 u_r}{\partial \theta^2} + \frac{\partial^2 u_r}{\partial z^2} - \frac{u_r}{r^2} - \frac{2}{r^2}\frac{\partial u_\theta}{\partial \theta}\right), \tag{2}$$

$$\frac{\partial u_\theta}{\partial t} + u_z\frac{\partial u_\theta}{\partial z} + u_r\frac{\partial u_\theta}{\partial r} + \frac{u_\theta}{r}\frac{\partial u_\theta}{\partial \theta} + \frac{u_\theta u_r}{r} = -\frac{1}{r}\frac{\partial p}{\partial \theta} + \frac{1}{Re}\left(\frac{\partial^2 u_\theta}{\partial r^2} + \frac{1}{r}\frac{\partial u_\theta}{\partial r} + \frac{1}{r^2}\frac{\partial^2 u_\theta}{\partial \theta^2} + \frac{\partial^2 u_\theta}{\partial z^2} - \frac{u_\theta}{r^2} + \frac{2}{r^2}\frac{\partial u_r}{\partial \theta}\right), \tag{3}$$

$$\frac{\partial u_z}{\partial z} + \frac{1}{r}\frac{\partial r u_r}{\partial r} + \frac{1}{r}\frac{\partial u_\theta}{\partial \theta} = 0. \tag{4}$$

The boundary conditions are

$$u_z = 0, u_r = 0, u_\theta = S \quad \text{for } z > 0, r = 1, \tag{5}$$

$$u_z \to 1, u_r = 0, u_\theta \to 0 \quad \text{for } z > 0, r \to \infty, \tag{6}$$

where u_z, u_r, u_θ are the non-dimensional velocities in axial, radial and azimuthal directions and p is the pressure. Re represents the Reynolds number which is the ratio of inertial forces to the viscous forces $Re = \frac{U_\infty a}{\nu}$ and the rotation rate S is the ratio of tangential velocity on the surface of cylinder to the free-stream velocity $S = \frac{\Omega a}{U_\infty}$. These are the two control parameters of the problem. Re appears explicitly in the equations (1)–(4) whereas S enters the problem as a boundary condition on u_θ in (5). This set of equations forms the starting point for both the basic flow and the linear stability analysis.

3 Basic flow

The flow around the rotating cylinder can be divided into two regions, an outer inviscid flow and a boundary layer near the wall which is caused due to the effect of friction. Basic flow computation consists in calculating steady and axisymmetric solution. Morever, when Re is large, boundary layer theory can be used, which takes advantage of the fact that the flow develops slowly along the axial direction in comparison with the evolution along the radial direction. Appropriate scalings based on boundary layer approximation are

$$R = r, \quad Z = \frac{z}{Re}, \tag{7}$$

$$U_z = u_z, \quad U_r = Ru_rRe, \quad U_\theta = Ru_\theta, \quad P = R^2 p, \tag{8}$$

where the factor of R in U_r, U_θ and P improves accuracy with the subsequent numerical calculations. The equations in these scaled variables along with the steady and axisymmetric assumptions are

$$U_z\frac{\partial U_z}{\partial Z}+\frac{U_r}{R}\frac{\partial U_z}{\partial R}=-\frac{1}{R^2}\frac{\partial P}{\partial Z}+\frac{\partial^2 U_z}{\partial R^2}+\frac{1}{R}\frac{\partial U_z}{\partial R}, \tag{9}$$

$$U_\theta^2=R\frac{\partial P}{\partial R}-2P, \tag{10}$$

$$U_z\frac{\partial U_\theta}{\partial Z}+\frac{U_r}{R}\frac{\partial U_\theta}{\partial R}=\frac{\partial^2 U_\theta}{\partial R^2}-\frac{1}{R}\frac{\partial U_\theta}{\partial R}, \tag{11}$$

$$\frac{\partial U_z}{\partial Z}+\frac{1}{R}\frac{\partial U_r}{\partial R}=0, \tag{12}$$

with the inlet and boundary conditions

$$U_z=1, U_\theta=0, U_r=0 \qquad \text{for } Z=0, \tag{13}$$

$$U_z=U_r=0, U_\theta=S \qquad \text{for } R=1, \tag{14}$$

$$U_z\to 1, U_\theta=0, P=0 \qquad \text{for } R\to\infty. \tag{15}$$

It can be seen that Re has been removed from the boundary layer equations by using the scaling. Though it is not possible to obtain similarity solutions as in the case of flat plate boundary layer, it is still possible to obtain a family of profiles for every value of Z. We can define another set of coordinates ζ, σ as

$$Z=\frac{1}{2}\zeta^2, \quad R=1+\zeta\sigma, \tag{16}$$

$$V_r=\zeta U_r, \quad V_z=U_z, \quad V_\theta=U_\theta, \quad \Pi=P. \tag{17}$$

This is better suited for the numerics as it removes the square-root singularity at $Z=0$ and reduces the inlet condition to a Blasius solution with an additional tangential velocity solution. This also allows us to take advantage of the $Z^{1/2}$ scaling of boundary layer thickness in a flat plate and the new radial coordinate σ is appropriately scaled with ζ since the boundary layer grows as Z increases. The infinite singularity in U_r at $Z=0$ is removed by multiplying a factor of ζ to it. The flow fields are then obtained by solving the boundary layer equations numerically in these transformed variables:

$$\zeta V_z\frac{\partial V_z}{\partial\zeta}+\left(\frac{V_r-\zeta}{R}-\sigma V_z\right)\frac{\partial V_z}{\partial\sigma}=\frac{1}{R^2}(\sigma\frac{\partial\Pi}{\partial\sigma}-\zeta\frac{\partial\Pi}{\partial\zeta})+\frac{\partial^2 V_z}{\partial\sigma^2}, \tag{18}$$

$$\frac{\zeta}{R}\left(V_\theta^2+2\Pi\right)=\frac{\partial\Pi}{\partial\sigma}, \tag{19}$$

$$\zeta V_z\frac{\partial V_\theta}{\partial\zeta}+\left(\frac{V_r+\zeta}{R}-\sigma V_z\right)\frac{\partial V_\theta}{\partial\sigma}=\frac{\partial^2 V_\theta}{\partial\sigma^2}, \tag{20}$$

$$\zeta\frac{\partial V_z}{\partial\zeta}-\sigma\frac{\partial V_z}{\partial\sigma}+\frac{1}{R}\frac{\partial V_r}{\partial\sigma}=0, \tag{21}$$

with the boundary conditions

$$V_z=V_r=0, V_\theta=S \qquad \text{for } \sigma=0, \tag{22}$$

$$V_z\to 1, V_\theta=0, \Pi=0 \qquad \text{for } \sigma\to\infty. \tag{23}$$

The mapped radial coordinate is discretized using Chebyshev collocation points with an algebraic transformation. The mapped axial direction ζ also extends from 0 to ∞ and is truncated at ζ_{max} and dis-

cretized using a finite difference scheme. At inlet the equations reduce to Blasius type of equations which are solved using a Newton–Raphson method. The boundary layer equations are then marched forward in ζ using an implicit Crank–Nicolson scheme where the equations are evaluated at the mid-point of two grid points. The resulting non-linear discretized boundary-layer equations are then solved using Newton–Raphson iteration by using the solution at previous axial step as an initial guess.

4 Linear stability analysis

To study the stability of this basic flow, the flow variables are first decomposed into a steady state (denoted by capital letters) obtained from the base flow calculation and a disturbance part as, e.g.,

$$u_z(z,r,\theta,t) = U_z(r,z) + \bar{u_z}(z,r,\theta,t). \tag{24}$$

The disturbance or the perturbation quantities $\bar{u_z}, \bar{u_r}, \bar{u_\theta}, \bar{p}$ are assumed to be infinitesimal and their addition to the steady flow represents a small change from the steady state. The stability analysis deals with understanding if the steady flow is stable/unstable to these perturbations. Using the flow variables in the form (24) in (1)–(4), we obtain the evolution equations for the perturbation. Since the perturbations are considered to be infinitesimal, the nonlinear terms are neglected. Another assumption is that the steady flow is locally parallel. This is justified since we know from the boundary layer theory that the steady state solution evolves slowly in z. Thus we can neglect the terms containing axial derivatives of the steady flow. Also since $U_z \gg U_r$ for the basic flow, terms containing U_r can be neglected.

Since the local flow is homogeneous in z and θ directions and also in time t one may resort to a normal-mode decomposition of the following form, e.g.,

$$\bar{u_z}(z,r,\theta,t) = \frac{1}{2}(\hat{v_z}(r)e^{\mathrm{i}(\alpha z + m\theta - \omega t)} + c.c.). \tag{25}$$

Here ω is the complex frequency, α is the streamwise wavenumber and m is the azimuthal mode number. Substituting these normal mode forms into the parallel linearized equations and dropping the hats in $\hat{v}$ results in

$$\mathrm{i}\alpha v_z + v_r' + \frac{1}{R}v_r + \frac{\mathrm{i}m}{R}v_\theta = 0, \tag{26}$$

$$\mathrm{i}\alpha(U_z - c)v_z + U_z' v_r + \frac{\mathrm{i}m\bar{U_\theta}}{R}v_z + \mathrm{i}\alpha p = \frac{1}{Re}\left[v_z'' + \frac{1}{R}v_z' - \left(\alpha^2 + \frac{m^2}{R^2}\right)v_z\right], \tag{27}$$

$$\begin{aligned}\mathrm{i}\alpha(U_z - c)v_r + \frac{\bar{U_\theta}}{R}(\mathrm{i}mv_r - 2v_\theta) + p' = \frac{1}{Re}\Bigg[v_r'' + \frac{1}{R}v_r' \\ - \left(\alpha^2 + \frac{m^2+1}{R^2}\right)v_r - \frac{2\mathrm{i}m}{R^2}v_\theta\Bigg],\end{aligned} \tag{28}$$

$$\begin{aligned}\mathrm{i}\alpha(U_z - c)v_\theta + \frac{\mathrm{i}m\bar{U_\theta}}{R}v_\theta + \left(\bar{U_\theta}' + \frac{\bar{U_\theta}}{R}\right)v_r + \frac{\mathrm{i}m}{R}p = \frac{1}{Re}\Bigg[v_\theta'' + \frac{1}{R}v_\theta' \\ - \left(\alpha^2 + \frac{m^2+1}{R^2}\right)v_\theta + \frac{2\mathrm{i}m}{R^2}v_r\Bigg].\end{aligned} \tag{29}$$

The complex phase velocity is denoted as c which is given by ω/α and the derivatives are with respect to R. Since U_θ in the basic flow has a factor of R, $\bar{U_\theta}$ is given by U_θ/R. The boundary conditions are

$$v_z(1) = v_r(1) = v_\theta(1) = 0, \tag{30}$$

$$v_z(\infty) = v_r(\infty) = v_\theta(\infty) = 0. \tag{31}$$

Temporal stability analysis deals with studying the evolution of perturbations in time. To study the temporal stability α, m are kept real and ω is considered to be complex. This results in an eigenvalue problem with ω being the eigenvalue and $X = \{v_z, v_r, v_\theta, p\}$ being the eigenvectors. The problem depends on input parameters α, Re, m, z, S and leads to the eigenvalues as a function of these parameters,

$$\omega = F(\alpha, Re, m, z, r, S). \tag{32}$$

This is known as the dispersion relation. A positive value of imaginary part of ω indicates that the perturbation grows in time which means the flow is unstable. The dispersion relation is numerically determined using the transformed ζ, σ coordinates which were introduced in the previous section, using the same Chebyshev discretization as for the basic flow. Pressure is numerically eliminated from stability equations using continuity equation to reduce the equations to a standard eigenvalue problem and also to reduce the size of the matrix in the eigenvalue problem. The code for linear stability has been validated against the neutral curve results for the non-rotating case by Tutty et al. (2002) and Vinod and Govindarajan (2012) and the results from Herrada et al. (2008) for the rotating case.

5 Results

5.1 Basic flow results

The problem of steady axisymmetric flow along a non-rotating cylinder has been previously studied by Tutty et al. (2002). Hence we compare the U_z results obtained for $S = 0$ at $Z = 0.001$ and 4.472 with our results.

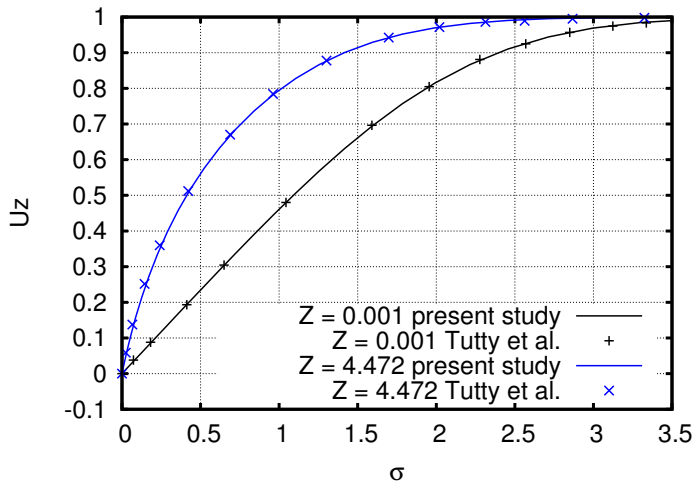

Figure 1: Comparison of U_z for $S = 0$ with Tutty et al. (2002)

From Figure 1, it can be seen that the results from our code are in good agreement with the results of Tutty et al. (2002). For the problem of rotating cylinder, the basic flow has been previously computed

for $S \leq 1$ by Herrada et al. (2008). They have plotted the skin friction along the cylinder for different values of S in their paper. The skin friction at a given Z is given by

$$\tau = \frac{\partial U_z(Z)}{\partial R} \mid_{R=1} \tag{33}$$

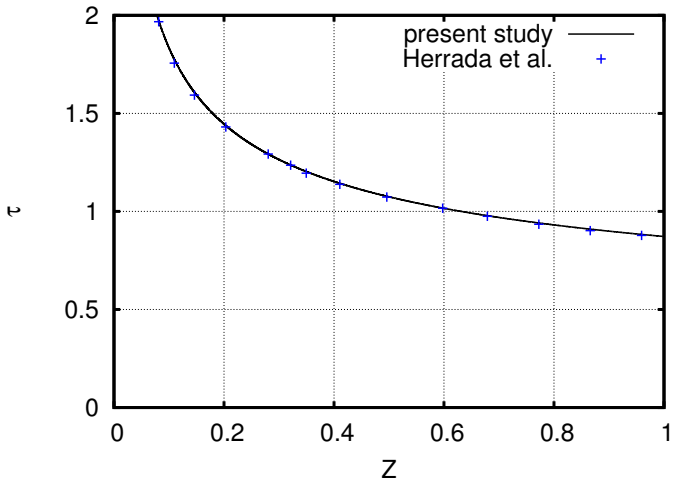

Figure 2: Comparison of skin friction τ for $S = 1$ with Herrada et al. (2008)

From Figure 2, it can be seen that the skin friction (or the shear) decreases as Z increases and the results for the case $S = 1$ are in perfect agreement with the results of Herrada et al. (2008). The velocity profiles for different values of Z (Figure 3b) show that at inlet the velocity profile is the same as the flat plate solution. As Z increases the flow profile deviates from Blasius flow. The profiles are plotted along σ which is scaled with boundary layer thickness to fit them in one graph. From Figure 3a we can see that as the rotation increases up to $S \leq 4.2$ the flow remains of Blasius type, but at S larger than this there is a wall–jet formation (see Petrov (1976)). This forms due to the favourable axial pressure gradient which is caused by the large S. Considering the wall-jet formation in the streamwise velocity profile we can define a measure of displacement thickness which is valid throughout the domain as

$$\delta = \int_1^\infty (|1 - U_z| dR) / \max(1, U_z^{max}). \tag{34}$$

If we plot this displacement thickness along Z for different values of S (Figure 4) it can be seen that, as Z increases, δ increases which means that the boundary layer continues to grow. As S increases the appearance of wall-jet causes δ to decrease.

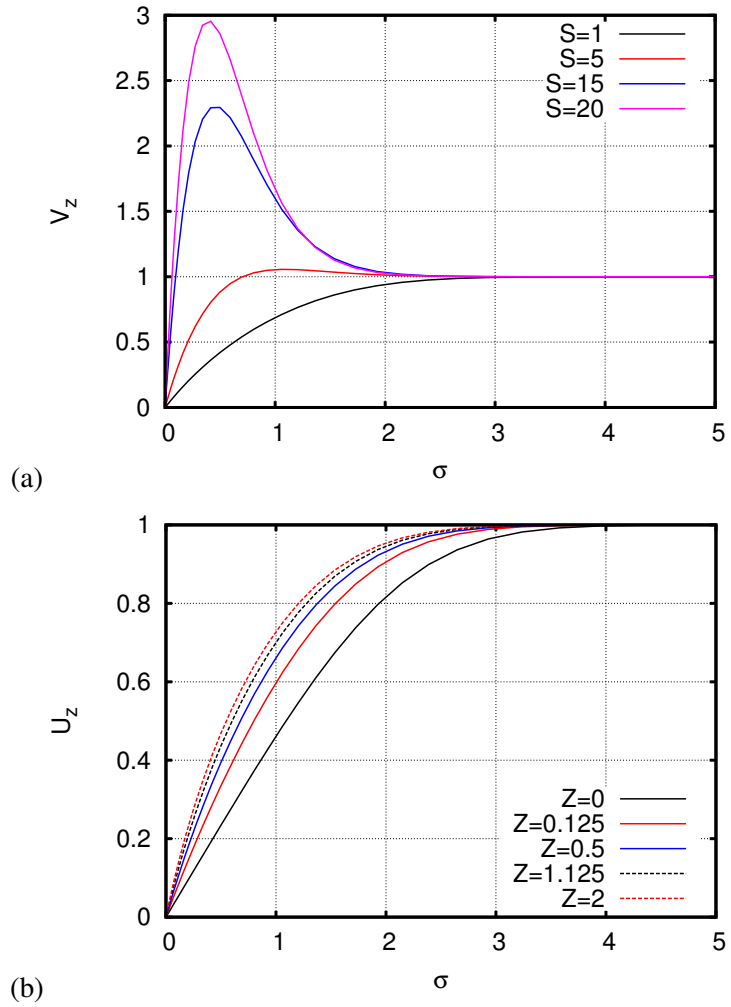

Figure 3: (a) Variation of axial velocity profile (U_z) at fixed axial position $Z = 0.5$ for different rotation rate (S). (b) Variation of U_z at fixed rotation rate $S = 0.1$ for increasing Z.

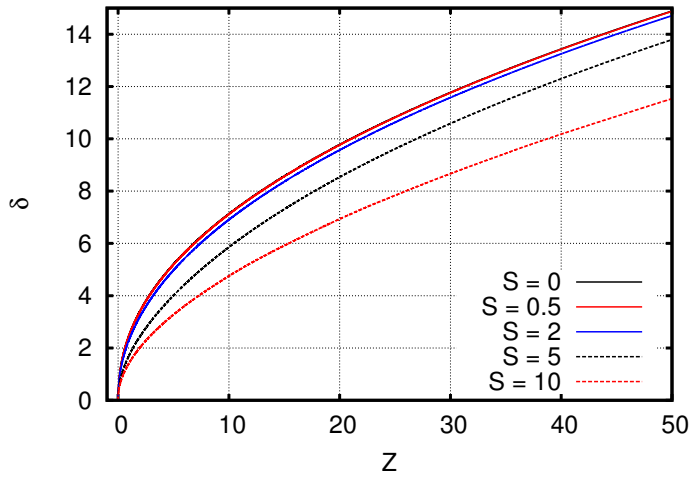

Figure 4: Variation of boundary layer thickness with Z and S.

5.2 Linear stability results

When the dispersion relation is numerically solved it leads to a discretized eigenspectrum. By looking at the eigenspectrum we can find out if there is any unstable mode ($\omega_i > 0$) for a given set of parameter. If we obtain the maximum of the growth rate over all axial wavenumbers for different values of Re and Z, the regions of instability can be identified. Then the curve describing the points where $\omega_i = 0$, known as the neutral curve, separates the unstable region from the stable region.

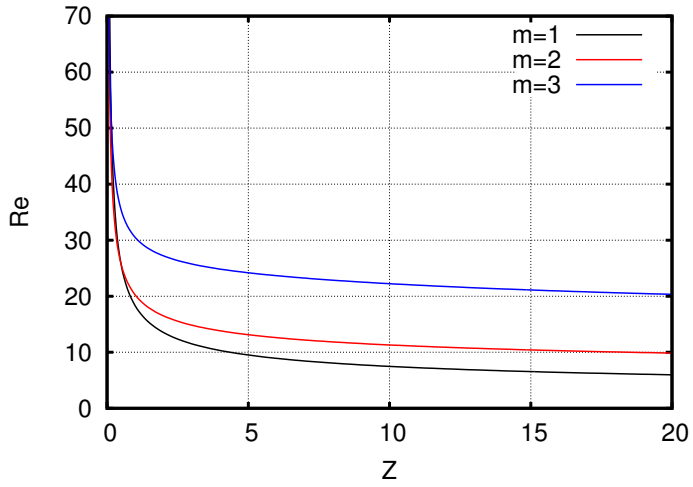

Figure 5: Critical curves for $S = 0.5$ for different values of m.

Such critical curves for increasing m at $S = 0.5$ (Figure 5) show that the mode $m = 1$ becomes unstable first (lower Re at a given Z) over large portion of Z compared to the other two. Thus we only consider $m = 1$ in the subsequent analysis since it becomes unstable at lower Re.

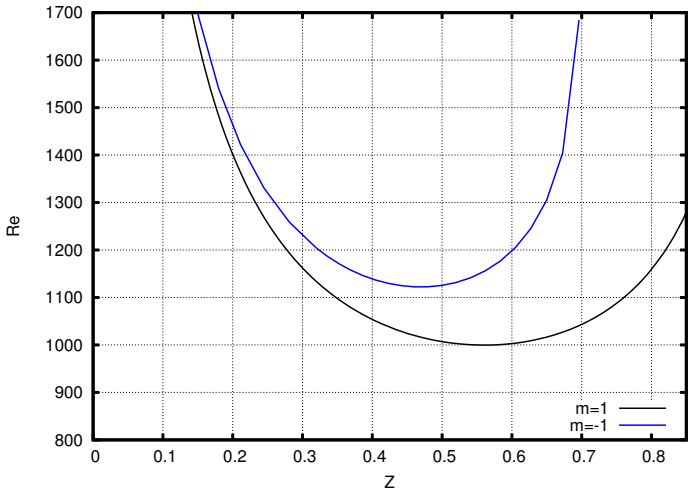

Figure 6: Neutral curves at $S = 0.0005$ for $m = 1$ and $m = -1$.

For non-rotating cylinder both positive and negative m give same growth rate due to reflection symmetry of the flow. By imposing a rotation this symmetry is broken and the growth rates are different. From Figure 6 it can be seen that even at a low value of S there is a significant shift in neutral curves for $m = 1$

and -1. The negative m's are found to be more stable than positive m and thus we only focus on m positive.

For the case of non-rotating cylinder with an axial flow the instability region in confined for a range of Z and the flow is stable far downstream. But when there is a small rotation on the cylinder, the flow becomes unstable even at larger Z as shown in Figure 7.

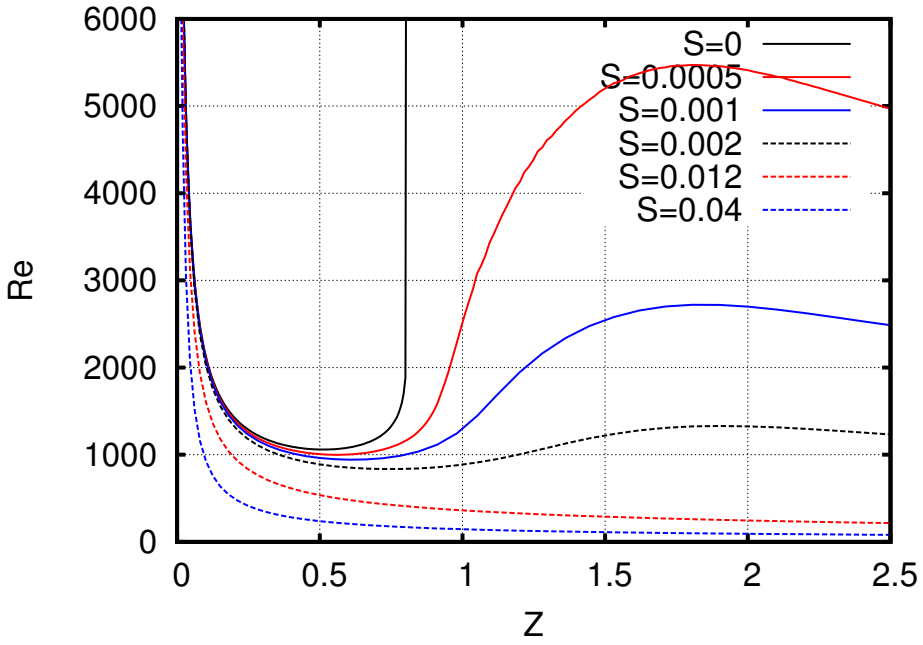

Figure 7: Neutral curves for $m = 1$ for small values of S.

By monitoring the spectrum, we find that the instability is not caused by new modes created due to rotation. Instead they are caused by the same modes from the non-rotating system which go unstable when there is rotation. It can be seen that even small value for rotation causes significant change in the stability characteristics. Hence we can think of small rotation of the cylinder as a small perturbation to the non-rotating case. The dispersion relation for the non-rotating problem can be represented as a standard eigenvalue problem given by

$$\omega_0 X_0 = A_0 X_0, \tag{35}$$

where ω_0 is the growth rate and X_0 is the set of velocities and pressure and A_0 is the square matrix which consists of the diffusion and advection terms. By introducing rotation, we simply add some more terms to the matrix A_0. Hence we can represent the rotating cylinder system as

$$\omega X = AX, \tag{36}$$

where A is the new matrix corresponding to rotation and ω, X are its eigenvalues and right eigenvectors.

By using a Taylor expansion of the eigenvalues, eigenvectors and A we can write

$$A = A_0 + SA_1 + S^2A_2 + \ldots, \tag{37}$$

$$\omega = \omega_0 + S\omega_1 + S^2\omega_2 + \ldots, \tag{38}$$

$$X = X_0 + SX_1 + S^2X_2 + \ldots \tag{39}$$

Using this in the dispersion relation (36) and only considering the first-order terms, after some algebraic steps, the first-order correction to ω_0 is given by

$$\omega_1 = \frac{Y_0^H A_1 X_0}{Y_0^H X_0}, \tag{40}$$

where Y_0 is the left eigenvector of the non-rotating case. Thus we can compute the eigenvalues for the rotating case ($\omega_0 + S\omega_1$) by just using the information from the non-rotating case for small S.

We have computed the eigenvalues of the rotating system and also the first- order correction to the non-rotating case using this perturbation method for $Z = 2$, $Re = 7500$, $\alpha = 0.004$, $m = 1$. We can see from Figure 8 that the perturbation method describes the eigenvalue behaviour reasonably well upto $S = 0.0005$. At larger S higher-order terms become significant and thus the first-order correction is less accurate.

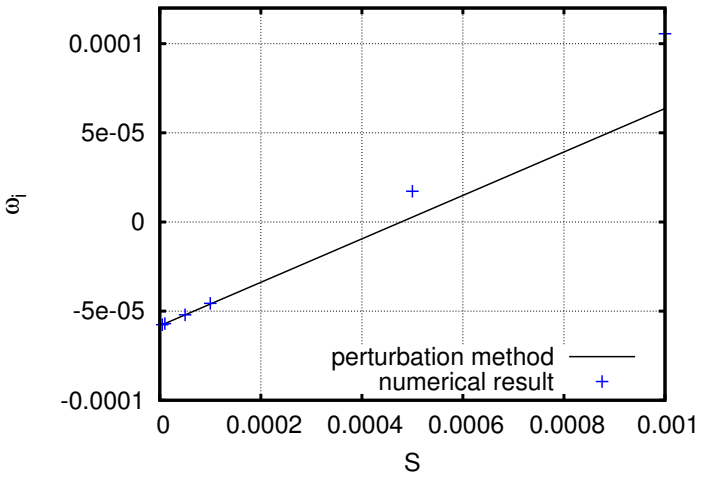

Figure 8: Comparison of eigenvalues obtained by numerical method and matrix perturbation theory for $Z = 2$, $Re = 7500$, $\alpha = 0.004$, $m = 1$.

For the non-rotating cylinder, there are weakly stable modes with small negative values of ω_i. Even small rotation can destabilize these modes, hence the significant shift in the neutral curves apparent in Figure 7. At large Z, this shift is particularly noticeable.

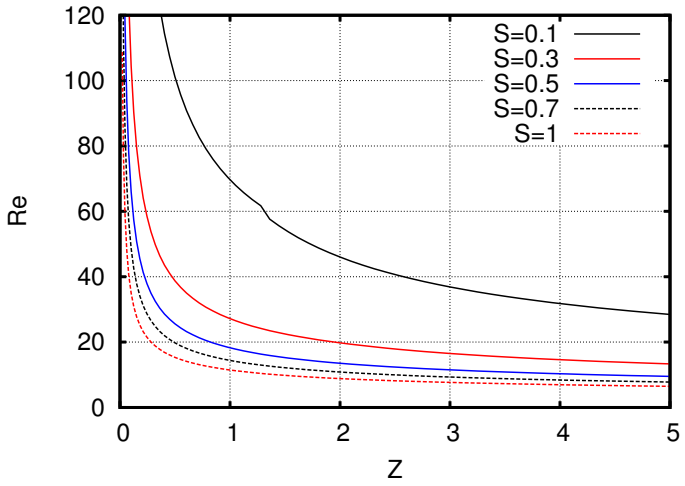

Figure 9: Neutral curves for increasing values of S at $m = 1$.

Critical curves computed for higher values of rotation rate (Figure 9) show that as S increases the flow becomes unstable at lower Re. At large Z from the asymptotic analysis it can be shown that the streamwise velocity U_z varies as $\ln(Z)^{-1}$ whereas U_θ is independent of Z. Thus the Re corresponding to the neutral curve also decreases as $\ln(Z)$ at large values of Z.

6 Conclusions

Based on the results we find that rotation creates a tangential velocity profile and modifies the streamwise velocity profiles from the non-rotating case. Rotation reduces the boundary thickness (δ) and when the rotation rate becomes large there is a large axial pressure gradient along the cylinder causing a wall-jet type of flow in the boundary layer where the velocity is larger than the free-stream velocity (Figure 3). Temporal stability analysis for the rotating cylinder shows that even small rotation can destabilize the flow. Rotation does not create new modes but destabilizes the weakly unstable modes of the non-rotating case, as quantified by the perturbation theory. It is mode $m = 1$ which becomes unstable first over most of the axial domain. As rotation increases the critical curves move to lower values of Re, indicating that the flow becomes more unstable. This work is a part of the ongoing research which also aims at studying the absolute stability characteristics of such a flow.

References

H Blasius. Grenzschichten in flüssigkeiten mit kleiner reibung. *Z Math Phys.*, 56, 1908.

MB Glauert and MJ Lighthill. The axisymmetric boundary layer on a long thin cylinder. *Proceedings of the Royal Society of London. Series A. Mathematical and Physical Sciences*, 230(1181):188–203, 1955.

MA Herrada, C Del Pino, and R Fernandez-Feria. Stability of the boundary layer flow on a long thin rotating cylinder. *Physics of Fluids*, 20(3):034105, 2008.

N.A. Jaffe and T.T. Okamura. The transverse curvature effect on the incompressible laminar boundary layer for longitudinal flow over a cylinder. *Zeitschrift für angewandte Mathematik und Physik ZAMP*, 19(4):564–574, 1968. ISSN 0044-2275.

GV Petrov. Boundary layer on a rotating cylinder in axial flow. *Journal of Applied Mechanics and Technical Physics*, 17(4):506–510, 1976.

R A Seban and R Bond. Skin-friction and heat-transfer characteristics of a laminar boundary layer on a cylinder in axial incompressible flow. *Journal of the Aeronautical Sciences (Institute of the Aeronautical Sciences)*, 18(10), 1951.

OR Tutty, WG Price, and AT Parsons. Boundary layer flow on a long thin cylinder. *Physics of Fluids*, 14:628, 2002.

N. Vinod and R. Govindarajan. Secondary instabilities in incompressible axisymmetric boundary layers: Effect of transverse curvature. *Journal of Fluids Engineering*, 134(2):024503, 2012.